11th International Symposium on Turbulence and Shear Flow Phenomena (TSFP11)
Southampton, UK, July 30 to August 2, 2019

EFFECT OF PRESSURE GRADIENTS ON THE DIFFERENT STAGES OF ROUGHNESS INDUCED BOUNDARY LAYER TRANSITION

Saikishan Suryanarayanan and David B. Goldstein
Aerospace Engineering and Engineering Mechanics, The University of Texas at Austin, Austin, TX 78712.
saikishan.suryanarayanan@gmail.com david@ices.utexas.edu

Alexandre R. Berger and Edward B. White
Aerospace Engineering, Texas A&M University, College Station, TX 77840.
bergeralexandre@tamu.edu ebw@tamu.edu

Garry Brown
Mechanical and Aerospace Engineering, Princeton University, Princeton, NJ 08544.
glb1873@msn.com

ABSTRACT

The physical mechanisms of roughness induced transition (RIT) in pressure gradient boundary layers are studied using direct numerical simulations. While recent investigations have provided a detailed understanding of RIT processes in zero pressure gradient boundary layers (Suryanarayanan *et al.*, 2019), it is unclear how these processes will be mechanistically altered in the presence of a locally accelerating or decelerating flow that can strain the vorticity field and create a net vorticity flux at the wall. Flow acceleration is imposed on specific regions of the flow evolution to understand how fundamental mechanisms in different stages of RIT are affected by pressure gradients using the complementary viewpoints of linear stability theory and vorticity dynamics. Preliminary results suggest that both lift-up and subsequent amplification of the unsteady perturbations are mitigated by flow acceleration.

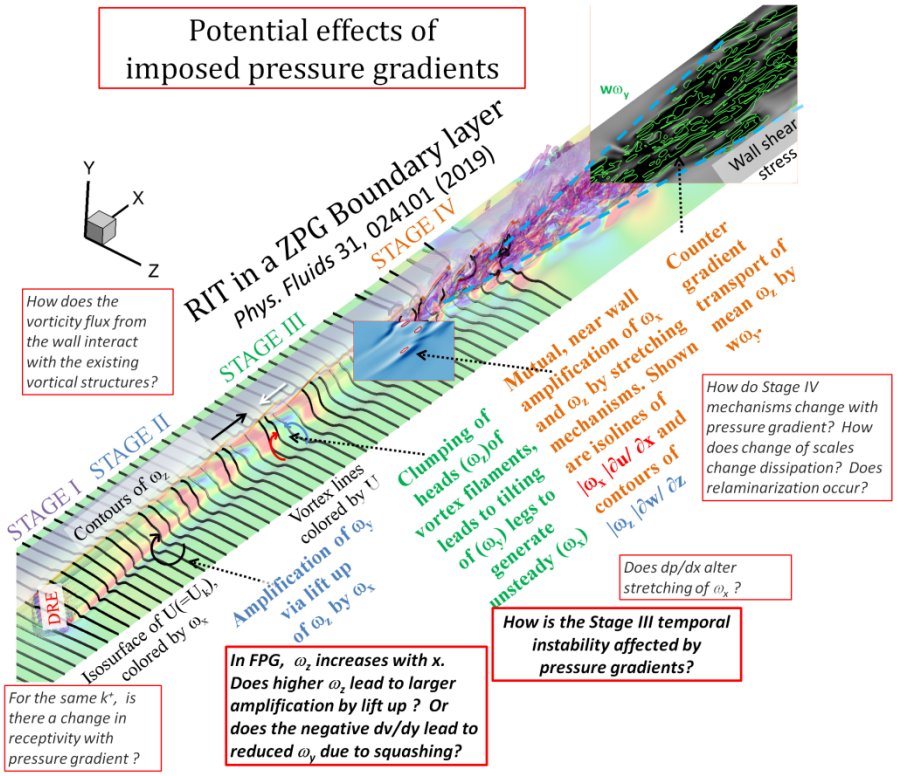

Figure 1. The mechanisms in the four stages of RIT in ZPG boundary layer and potential ways by which an imposed pressure gradient could influence the different mechanisms (red boxes).This paper aims to address the questions shown in **bold**.

BACKGROUND

Recent results from immersed boundary direct numerical simulations (Suryanarayanan *et al.*, 2017a, 2019), supported by matched experiments (Berger *et al.*, 2017, Suryanarayanan *et al.*, 2017b), have revealed that RIT in zero pressure gradient (ZPG) boundary layers have four distinct stages (see Fig. 1). The vorticity perturbations generated by the interaction of the incoming boundary layer

with the discrete roughness element (**Stage I,** '*receptivity*') undergo, initially, a steady spatial amplification (**Stage II,** '*transient growth*') via the lift up of the spanwise vorticity (ω_z) by the streamwise vorticity (ω_x) perturbations to amplify the spanwise gradients (or wall normal vorticity ω_y). In **Stage III** ('*secondary instability*'), high-frequency disturbances amplify along the high-shear region on top of the three-dimensional vortical structure. The dominant frequency of these perturbations is predicted by an application of linear stability theory to the distorted steady base flow calculated by DNS. This approach has been demonstrated by Berger *et al.* (2017) using a code developed by Monschke (2015).

In this work, similar calculations have been performed. Figure 2 compares the results of an inviscid, parallel, linear stability analysis of the DNS time-average base flow at x/k = 22 to u'_{rms} fluctuations calculated by DNS at x/k = 35. The stability analysis is the 2D, inviscid, spatial eigen value calculation developed by Monschke (2015). It is found that both the perturbation frequency (LST: $f = 0.124\ \omega_{z0}$; DNS: f ~ 0.13 ω_{z0}) and mode shape (Fig.2) correspond well to DNS calculations.

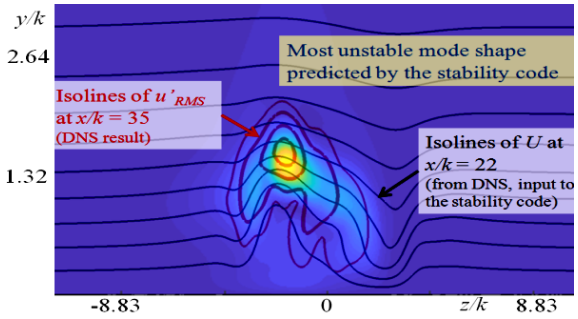

Figure 2. Comparison of mode shape predictions of LST of the DNS time-average flow field at x/k = 22 with the DNS u'_{rms} amplitudes at x/k = 35 in the DNS for the ZPG case. The LST frequency is $f = 0.124\ \omega_{z0}$ which is the more unstable of two unstable modes that exist for these conditions.

The evolution following the modal amplification of linear-amplitude unsteady disturbances is dominated by the mutual amplification of streamwise and spanwise vorticity via a mutual stretching process. This leads to locally intense vortical structures, such as hairpin vortices, that lead to chaotic behavior and breakdown to turbulence (**Stage IV**). The spanwise spreading of the turbulent region by local processes at the edge of the wedge that can be explained by vorticity dynamics (Goldstein *et al.*, 2017) and increased wall shear stress are observed in this Stage. The observed correlation of $\overline{w\,\omega_y}$, ω_x^2 and wall shear stress, suggests the following explanation for the increased wall shear stress. Since ω_x^2 creates both the spanwise velocity w (by Biot-Savart induction) and ω_y (by local lift up of ω_z), it leads to the correlation of w and ω_y which is responsible for the counter gradient transport of mean spanwise vorticity toward the wall, causing the increased wall shear stress. This last stage has parallels in turbulent channel flow dynamics (Brown *et al.*, 2015) and with observations in relaminarizing boundary layers (Brown *et al.*, 2017). While the applicability of RIT mechanisms to other bypass transition scenarios is a topic of concurrent research (Goldstein *et al.*, 2018), there are practical benefits to in-depth analyses of RIT, including the understanding of the mechanisms that have lead to novel ways of mitigating RIT (Sharma *et al.*, 2014, Kuester *et al.*, 2014, Suryanarayanan *et al.*, 2017b, 2018).

A target application of RIT control is on the leading edge of low-speed aircraft wings in which bypass transition caused by built-in or environmentally accumulated roughness is a well-known route to early transition. However, the favorable pressure gradient (FPG) of the aircraft wing leading edge may significantly alter the ZPG picture of RIT. It may be possible that for small roughness elements, the velocity distribution in the boundary layer is nearly linear till roughness height k, and that RIT depends only on $k^+ = u_\tau k/\nu$, where u_τ is the friction velocity. This was perhaps first suggested by S. Goldstein in 1936 (see Schlichting 1979). On a similar note, Loftin (1945) suggested the critical height of a given roughness shape depended on Re_{kk} (= $U_k k/\nu$,approximately equal to k^{+2} close to the wall) and that protuberances are more likely to cause RIT than incised scratches. These ideas were supported by recent work (Suryanarayanan et al., 2017a) that showed near identical RIT processes for zero pressure gradient (ZPG) boundary layer and Couette flow (which, crucially, is stable to all linear perturbations) with the same k^+. However, pressure gradient not only leads to change in the shape of the boundary layer profile but also a streamwise variation of the free stream speed, and hence the near wall vorticity field. The majority of the work done on RIT, including in our own group and the control strategies we have developed, were all in a ZPG setting. Ehrmann *et al.* (2013) observed that that the critical value of Re_{kk} hardly changes upon varying angle of attack from –4° to +3° of a 63-418 airfoil. While this may suggest that pressure gradients may not independently enter the problem when scaled by near wall or roughness parameters, detailed mechanisms and the dependence of the actual transition location have not been examined. While bulk measurements have been used to examine the empirical effect of pressure gradient on RIT since the 1940s (see Abbott & Von Doenhoff, 1959), and pressure gradient effects have been used in transition models (e.g. Van Driest, 1967), it is essential to examine the vorticity dynamics of the different stages and the effect of pressure gradients on each of the underlying mechanisms to be able to provide more accurate predictions, or more importantly, determine ways of interfering with them to achieve transition control.

While a FPG is known to delay or suppress transition in 2D boundary layers, it is important to note that it leads to increasing wall vorticity and generates a vorticity flux from the wall, likely enhancing the amplification by lift-up in Stage II of RIT. But a FPG may also increase dissipation. Different processes in Stages III and IV may perhaps be enhanced or disrupted by the FPG. These possibilities are shown in Fig.1.The major questions that need to be addressed are: How can the results on RIT mechanisms and control strategies from a ZPG boundary layer be extrapolated to favorable (FPG) and adverse pressure

gradient (APG) boundary layers? Which stages of RIT solely depend on near wall vorticity and length scales? Can the role of impressed pressure gradients be understood purely in terms of wall vorticity fluxes? How well can a local, linear stability theory predict growth of perturbations in Stage III? This paper aims to provide some insight based on preliminary simulations of RIT with pressure gradients.

COMPUTATIONAL SETUP

The present work aims to address the above questions using the immersed boundary, pseudo spectral solver (Goldstein *et al.*1993, 1995) used in ZPG simulations with appropriate modifications. The base solver has been used for a wide range of simulations, including for boundary layer transition studies with discrete (Sharma et al 2014, Suryanarayanan et al 2017a) and distributed roughness (Kuester *et al.* 2014), examination of turbulent wedge evolution (Goldstein *et al.* 2017), turbulent spots over riblets (Strand, 2007) among others. Many of these studies include favorable comparisons with matched experiments.

A. Schematic of the physical setup of RIT in PG flows

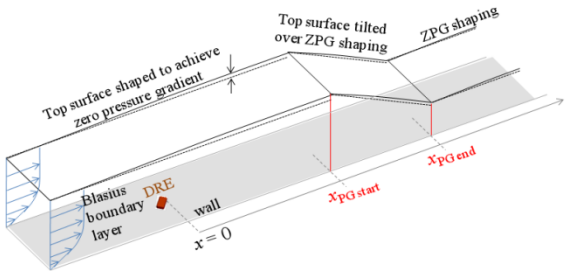

B. 2D calculation without roughness. k refers to the height of the roughness in the 3D calculation that uses this as initial condition.

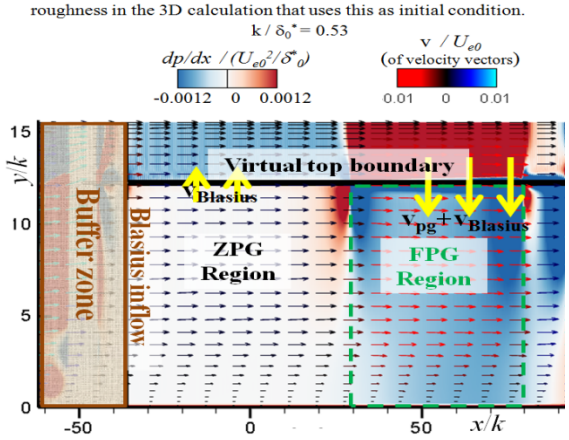

Figure 3. Simulation setup and steady state solution of a favorable pressure gradient simulation at which a pressure gradient of $-0.0008\ U_{e0}^2/\delta_0^*$ is applied from $x/k = 29$ to 80. Shown are contours of pressure gradient and velocity vectors colored by vertical velocity.

The present setup is broadly similar, except that at the virtual top boundary, the applied forces ensure velocity components that are a sum of the Blasius far field velocity and an additional term due to the applied pressure gradient. The added term is calculated by an inviscid approximation of flow through a channel (of height H - δ^*_0, where H is the height of the virtual top surface from the wall and $\delta^*_0$is the nominal displacement thickness of the boundary layer at the roughness location) with a top plate inclined to the flow. For each case, a two-dimensional calculation is performed (without any roughness) and the steady state obtained is used as an initial condition for the 3D simulation with a discrete roughness (of the same geometry as the ZPG case of Suryanarayanan et al., 2019) with the same virtual top boundary conditions.

The 2D simulations (Fig. 3) show that the pressure gradient applied by forcing the velocity on the virtual top boundary extends to the lower wall (after a short streamwise delay) consistent with the boundary layer theory. (It was also observed that a small (~2.5%) increase in U_e can lead to a substantial (~40%) increase in ω_z near the wall).

There are two broad sets of cases that are considered in this paper. The first set (k13) is one in which the DRE does not cause transition in the ZPG case. The Reynolds number based on the nominal incoming boundary layer displacement thickness, $Re_{\delta 0^*}$, for these cases is about 1220 and the Reynolds number based on the DRE height and the velocity of the undisturbed boundary layer at that height, Re_{kk} is about 190 ($k^+ = u_\tau k/\nu = 13.8$). The k13 simulations are performed using 768 x 128 x 384 grid points in the streamwise (x), wall normal (y) and spanwise (z) directions, respectively, covering a domain of dimensions $82.2\delta_0^* \times 20.6\delta_0^* \times 8.22\delta_0^*$. The second set of simulations (k15) are performed at a higher Reynolds number at which the DRE is observed to cause transition about $100k$ downstream in the ZPG case. The roughness shape, δ_0^* andU_{e0} are unaltered from the k13 case. These simulations have $Re_{\delta 0}^* \approx 1480$, and $k^+ \approx 15.15$, and are performed using 768 x 128 x 192 grid points covering a domain of dimensions $164.4\delta_0^* \times 20.6\delta_0^* \times 8.22\delta_0^*$.The value of $k/\delta_0^* = 0.53$ in both sets of simulations.

ROLE OF PRESSURE GRADIENTS IN ALTERING (STAGE II) LIFT-UP / TRANSIENT GROWTH

Three k13 simulations, one with FPG ($dp/dx = -0.0008\ U_{e0}^2/\delta_0^*$), second with APG ($+0.0003\ U_{e0}^2/\delta_0^*$) and the third baseline ZPG case, are performed. The pressure gradient is applied from $x/k = 29$ to 80 downstream of the roughness for both the FPG and APG cases. It is observed that the flow does not transition and remains steady for all three cases and the solution is broadly similar across cases. A closer examination reveals differences in the evolution of the different vorticity components (Figure 4). It can be seen from Fig.4A that ω_x^2 is initially (slightly) larger for FPG case. This is expected because of the stretching of ω_x by du/dx. The evolution of ω_y^2shows an opposite trend with pressure gradient - a favorable pressure gradient leads to lower values of (y-z) plane integrated ω_y^2 while an adverse pressure gradient causes a larger value. The reason for this observation becomes clear on examining the ω_y^2 flux balance in the region where the pressure gradient is applied. It can be seen that $\omega_y^2\,\partial v/\partial y$ becomes large and negative for the favorable pressure gradient case (note, by continuity, $\partial v/\partial y = -\partial u/\partial x$), and this 'squashing' is responsible for

the decrease in ω_y^2 with pressure gradient. While none of the three simulations lead to transition or any noticeable unsteadiness at steady state, they provide important insights into the effect of pressure gradient in Stage II of RIT - a favorable pressure gradient leads to a smaller values of 'effective lift-up' and thus is possibly less prone to the onset of stage III temporal oscillations.

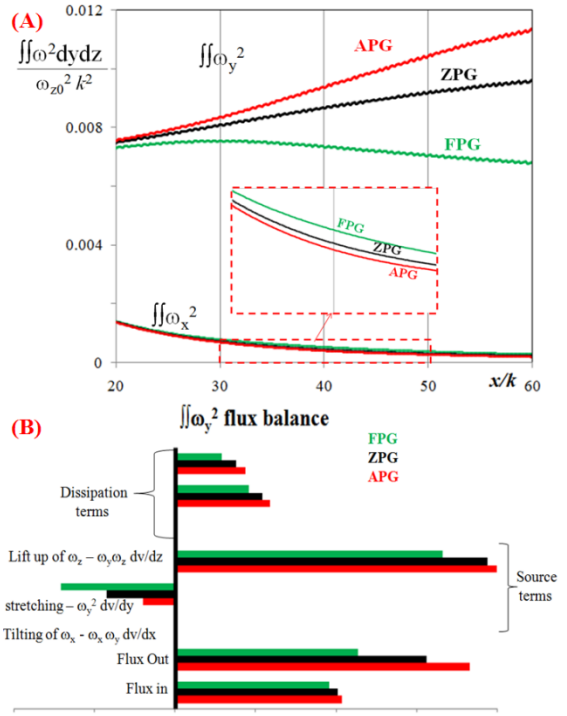

Figure 4A. The effect of pressure gradient in altering the streamwise evolution of plane integrated ω_x^2 and ω_y^2 downstream of the DRE in k13 simulations. **B.** Effect of pressure gradients in altering different terms of the ω_y^2 flux balance in the control volume downstream (x/k = 29 to 80) of the DRE.

ROLE OF PRESSURE GRADIENTS IN SUBSEQUENT EVOLUTION (STAGES III & IV)

Simulations are performed at $k+$ = 15.15 for two different values of favorable pressure gradients and one value of adverse pressure gradient, in addition to the base ZPG case. The pressure gradient is either applied from x/k = 6 to 99 (covering Stages II and III) or from x/k = 46 to 139 (predominantly Stages III and IV), leading to a total of 7 distinct cases. Snapshots of results from these calculations are shown in Fig. 5.

The first set of cases show that favorable pressure gradient suppresses transition and adverse pressure gradients advance the transition location. The strong suction causes a difference in the geometry/inclination of the hairpins in the wedge in the APG simulations. On the other hand, if the favorable pressure gradient is strong enough it can prevent transition. The flow remains entirely steady when the pressure gradient is applied between 6k and 99k for both the values of FPG considered here. Thus it is possible to alter the critical Re_{kk} with favorable pressure gradients applied downstream of the roughness, even for the same inflow. These results are consistent with the k13 simulations which showed that even though a favorable pressure gradient amplified ω_x^2 (which nevertheless can decay on its own) the net amplification of ω_y^2 during Stage II is reduced with pressure gradient, and a large enough ω_y^2 is necessary to sustain the growth of the unsteady perturbations.

In order to examine whether for the same Stages I and II, how the evolution is altered in Stage III and beyond, cases where the pressure gradient is applied further downstream are considered. The results are broadly consistent with the previous set of cases - a strong favorable pressure gradient can still entirely suppress transition even when applied beyond x/k ~ 50, though transition is not suppressed by the lower magnitude FPG in this case. It has to be noted that there is an overlap of the mechanisms in Stage II and III at this value of x/k, so some caution is required in interpretation of these results. Ongoing work involves the examination of the effect of pressure gradient on the mode shapes, frequencies and growth exponents by an application of LST for a given base velocity profile, and comparison with the DNS results. Time averaged wall shear stress and u'_{RMS} isosurfaces of the FPG and APG cases are compared with the baseline ZPG case in Fig. 6. The evolution of wall shear stress suggest that favorable pressure gradients may reduce the spanwise spread angle of the turbulent wedge and that adverse pressure gradient has the opposite effect. A similar observation can be made based on turbulence intensity. Future work would include simulations specifically tailored to study the effect of pressure gradients on the development of turbulent wedge and examine the results from a vorticity point of view along the lines of Goldstein *et al.* (2017). Separately, investigations of Stage IV mechanisms including the possibility of relaminarization (as opposed to prevention of transition that has been demonstrated here) by an application of strong FPG on a fully developed turbulent wedge are being carried out.

SUMMARY

The preliminary DNS presented here show that the role of pressure gradients on specific mechanisms of RIT can be studied within the present numerical setup. For a given set of perturbations generated by the interaction of the DRE with an incoming boundary layer, the present DNS have demonstrated that the transient growth in Stage II is reduced by FPG and enhanced by APG. The squashing of the wall normal vorticity by dv/dy is responsible for this effect which has the potential to advance or prevent transition. Application of pressure gradients at a downstream location leads to similar trend, with interesting observations on wall shear stress evolution and wedge spreading that demand further investigation.

ACKNOWLEGEMENTS

The authors gratefully acknowledge the support of the U.S. Air Force Office of Scientific Research through grant numbers FA9550-15-1-0345 and FA9550-19-1-0145. The authors also thank Dr. Jason Monschke for his assistance in performing linear stability calculations.

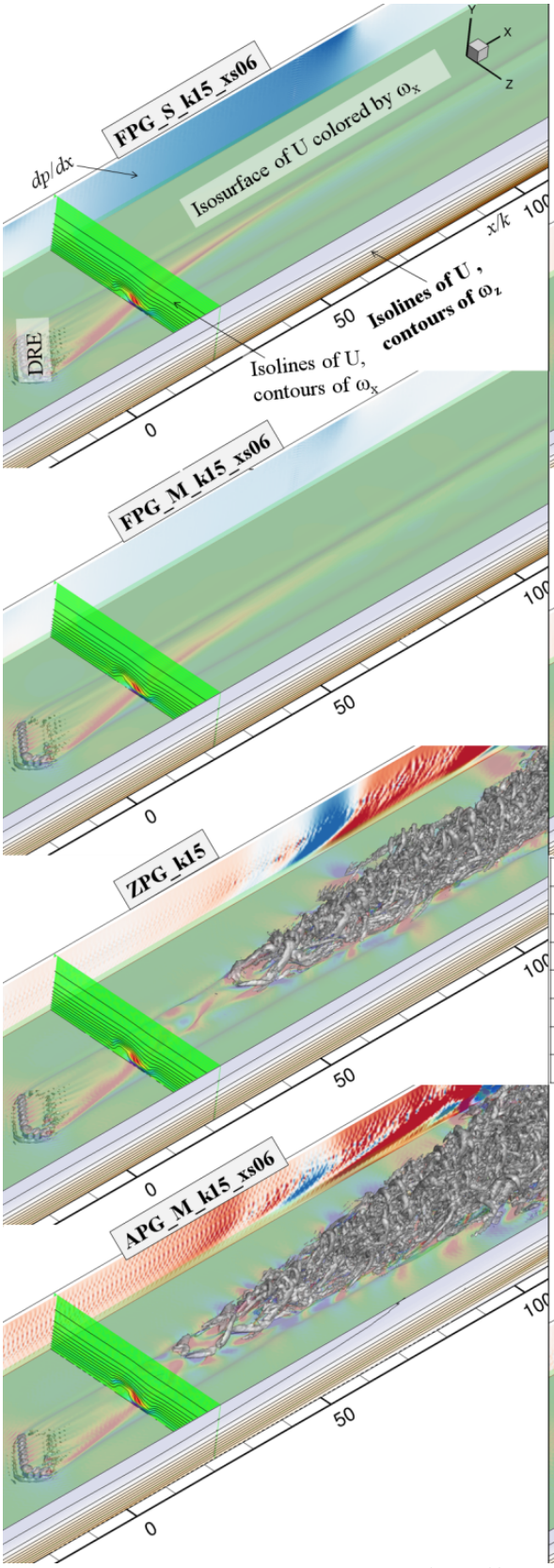

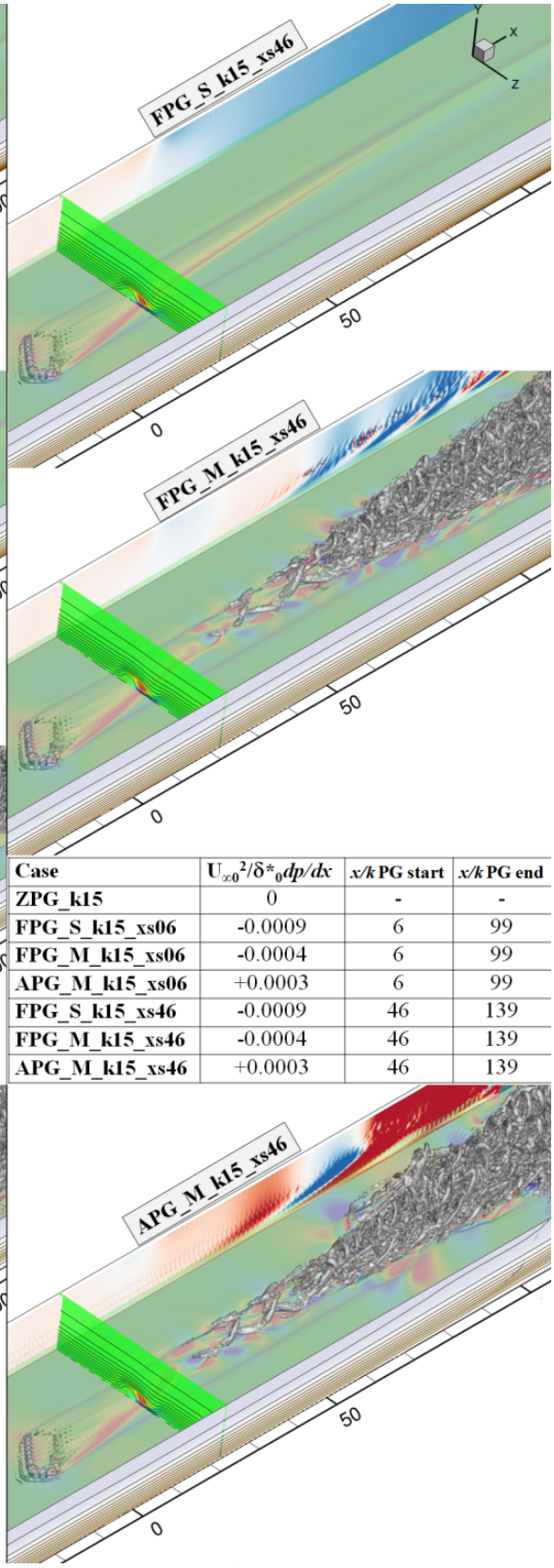

Case	$U_{\infty 0}^2/\delta^*_0 dp/dx$	*x/k* PG start	*x/k* PG end
ZPG_k15	0	-	-
FPG_S_k15_xs06	-0.0009	6	99
FPG_M_k15_xs06	-0.0004	6	99
APG_M_k15_xs06	+0.0003	6	99
FPG_S_k15_xs46	-0.0009	46	139
FPG_M_k15_xs46	-0.0004	46	139
APG_M_k15_xs46	+0.0003	46	139

Figure 5. Comparison of k15 cases (instantaneous snapshots).

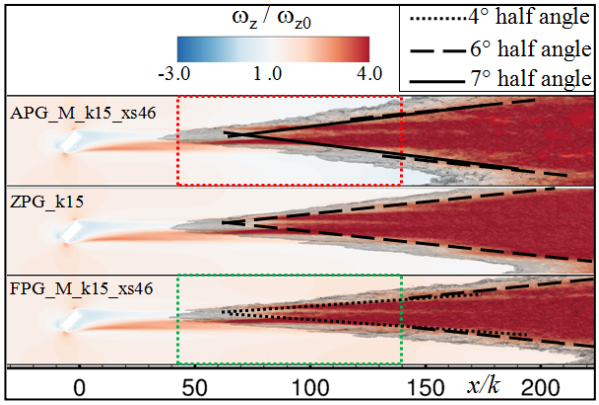

Figure 6. Time averaged wall shear stress contours (red-blue). Also shown is a translucent isosurface of $u'_{RMS} = 0.05\ U_{e0}$.

REFERENCES

Abbott, I.H. and Von Doenhoff, A.E., 1959. *Theory of Wing Sections, Including a Summary of Airfoil Data*. Dover Publications.

Berger, A. R., McMillan, M.N., White, E. B., Suryanarayanan, S. & Goldstein, D.B., 2017. Suppression of Transition Behind a Discrete Roughness Element Using a Downstream Element. *10th Intl. Symp. on Turbulence and Shear Flow Phenomena* (TSFP10), Chicago-IL, USA.

Brown, G.L., Lee, M. and Moser, R.D, 2015. Vorticity transport: the transfer of viscous stress to Reynolds stress in turbulent channel flow. *9th International Symposium on Turbulence and Shear Flow Phenomena* (TSFP9), Melbourne, Australia.

Brown, G.L., Patwardhan, S.S. and Ramesh, O.N., 2017. Re-laminarization and re-transition of a turbulent boundary layer from a vorticity point of view. *10th Intl. Symp. on Turbulence and Shear Flow Phenomena* (TSFP10), Chicago-IL, USA.

Ehrmann, R.S., White, E.B., Maniaci, D.C., Chow, R., Langel, C.M. and Van Dam, C.P., 2013. Realistic leading-edge roughness effects on airfoil performance. AIAA Paper 2013-2800.

Goldstein, D.B, Chu, J. and Brown, G.L, 2017. Lateral Spreading Mechanism of a Turbulent Spot and a Turbulent Wedge. *Flow, Turbulence and Combustion*, 98(1),pp.21-35.

Goldstein, D.B, Handler, R. and Sirovich, L., 1993. Modeling a no-slip flow boundary with an external force field. *J. Comput. Phys*., 105(2), pp.354-366.

Goldstein, D.B, Handler, R. and Sirovich, L., 1995. Direct numerical simulation of turbulent flow over a modeled riblet covered surface. *J. Fluid Mech.*, 302, pp.333-376.

Goldstein, D.B. Suryanarayanan, S.& Brown, G.L., 2018.On the final stages of transition to turbulence in wall bounded flows. To be presented at the *71st Annual Meeting of the APS Division of Fluid Dynamics* (APS DFD 2018), November 18–20, 2018, Atlanta, Georgia.

Kuester, M.S., Sharma, A., White, E.B., Goldstein, D.B. and Brown, G., 2014. Distributed Roughness Shielding in a Blasius Boundary Layer. AIAA 2014-2888. In *44th AIAA Fluid Dynamics Conference*.

Loftin, L.K., JR., 1945. Effects of specific types of surface roughness on boundary-layer Transition. NACA ACR L5J29a, 1945 (Wartime Rept. No. L-48).

Monschke, J., 2015. *Most-Critical Transient Disturbances,* Ph.D. Texas A&M University.

Schlichting, H., 1979. *Boundary-layer theory*. McGraw-Hill.

Sharma, A., Drews, S., Kuester, M.S., Goldstein, D.B. and White, E.B., 2014. Evolution of disturbances due to distributed surface roughness in laminar boundary layers. AIAA 2014-0235. In *52nd Aerospace Sciences Meeting.*

Strand, J., 2007. DNS of surface textures to control the growth of turbulent spots. Masters Thesis, The University of Texas at Austin, Dec. 2007.

Suryanarayanan, S., Goldstein D.B. and Brown, G.L.,2017a. Roughness Induced Transition In Wall Bounded Flow: A Vorticity Point Of View, *Tenth International Symposium on Turbulence and Shear Flow Phenomena* (TSFP10), July 6-9, 2017, Swissotel, Chicago-IL, USA.

Suryanarayanan, S., Goldstein, D.B., Brown, G.L., Berger, A.R. and White, E.B., 2017b.On the Mechanics and Control of Boundary Layer Transition induced by Discrete Roughness Elements. AIAA 2017-0307. In *55th AIAA Aerospace Sciences Meeting.*

Suryanarayanan, S., Goldstein, D.B., Berger, A.R., White, E.B. & Brown, G.L., 2018. Toward A Generalized Roughness-Induced-Transition Mitigation Strategy Using A Streamwise Array of 2D Flat Strips. AIAA 2018-3077.In *2018 Fluid Dynamics Conference*.

Suryanarayanan, S., Goldstein, D.B and Brown, G.L., 2019. Roughness Induced Transition In Wall Bounded Flow:A Vorticity Point Of View. *Phys. Fluids* **31**, 024101.

Van Driest, E. R., Blumer, C. B., and Wells, C. S., Jr., "Boundary Layer Transition on Blunt Bodies—Effects of Roughness," *AIAA J.*, **5**, Oct. 1967, pp. 1913–1915.